

Electronic Supplementary Information

Utilization of process analytical technologies (PAT) as a versatile in situ monitoring tool for kinetic evaluation of photocatalytic reactions

Martin Rößler, Philipp U. Huth, and Marcel A. Liauw

Institut für Technische und Makromolekulare Chemie, RWTH Aachen University, Worringerweg 1, 52074 Aachen, Germany. *E-Mail: liauw@itmc.rwth-aachen.de, Tel: +49 (0) 241 80 26470

1. General Information

4-(methoxythiophenol) (97%) (4-MTP) and bis(4-methoxyphenyl)disulfide (98%) (4-MPD) were provided by ABCR. *N,N,N',N'*-Tetramethylethylenediamin (99 %) (TMEDA), eosin y (dye content > 85 %) (EY) and ethanol (> 99.8%, HPCL grade) were provided by Sigma-Aldrich. All chemicals were used without further purification.

2. Monitoring Setup

All reactions were conducted in a home-designed photoreactor setup including a glass vessel (Fig. S1) and an illumination unit. For reproducible results, the glass vessel was fixed in the 3D-printed illumination unit. With this, a constant distance between the vessel and the irradiation source was ensured. Irradiation of the sample was conducted via 12 high power LEDs (Nichia NCSG219B-V1) distributed on six LED plates in a circular arrangement around the reactor. The LEDs were wired in row and driven by a constant current of 0.5 A. The light intensity was controlled by a microcontroller via puls width modulation (PWM). Cooling was conducted with compressed air. Stirring was conducted by a stirrer hot plate (Heidolph, Schwabach, Germany) and a customized magnetic stirrer made from Teflon (Fig. S1).

All relevant measures of the glass reactor are listed in Fig. S1. For monitoring, suitable immersion probes were inserted in a 45° angle and fixed by GL-screw connectors (Bohlender, Grünsfeld, Germany). Oxygen with a constant pressure was directly introduced to the liquid phase using a FEP capillary (OD 1/8", Bohlender, Grünsfeld, Germany).

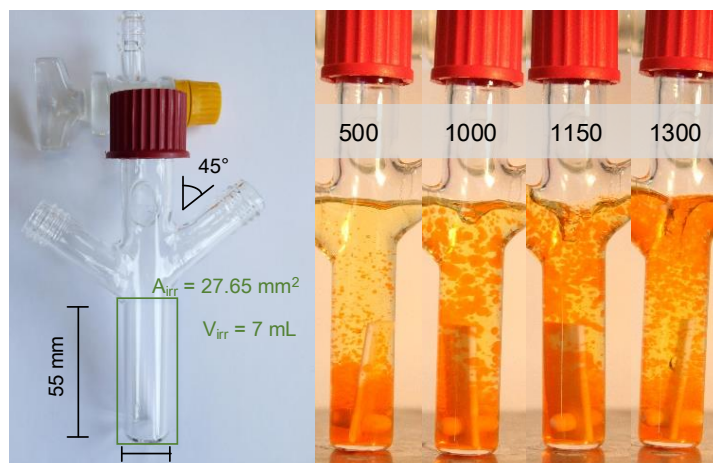


Fig. S1: Representation of the home-designed photoreactor to study the kinetics of photocatalytic reactions (left). Visualisation of the stirring efficiency with the home-designed stirrer at various stirring speeds in a biphasic mixture (right).

In situ Raman spectra were recorded using a RXN2 spectrometer (Kaiser Optical Systems, Lille, France). The spectrometer was equipped with a 785 nm excitation laser and spectra were acquired using an immersion probe with a short focus optic. For reactions with *in situ* Raman, the reactor was covered from ambient light to reduce artefacts occurring from stray light (Fig. S2). *In situ* UV/Vis (fluorescence) spectra were recorded by an ATR-probe (type KATANA, Hellma Analytics, Mülheim/R., Germany) coupled to an AvaSpec 2048 spectrometer (Avantes, Apeldoorn, Netherlands). Mid-IR spectra were recorded using an MATRIX-MF spectrometer (Bruker Optik, Ettlingen, Germany) coupled to an ATR immersion probe (IN350-T, infrared fiber sensors, Aachen, Germany) with a Hastelloy shaft and internal reflection element made of diamond.



Fig. S2: Integration of compatible immersion probes in the photoreactor (left and middle). Light cover for Raman application (right).

3. Photocatalytic oxidation of 4-MTP to 4-MPD

Photocatalytic oxidation reactions were performed in the previously described reactor setup applying *in situ* Raman spectroscopy. Under standard conditions the reaction solution contained 0.2 M 4-MTP, 0.2 M TMEDA and 0.00015 M EY that were filled up to a total volume of 10 mL with ethanol. After dissolving all reactants, the reaction mixture was transferred to the reactor. Prior to irradiation all reaction solutions were saturated with oxygen in the dark for 5 Min. Under standard conditions, the reaction was performed at a stirring rate of 1300 rpm and a constant oxygen pressure of 2 bar.

4. Absorption Study EY

Offline absorption spectra were recorded using a *MultiSpec* (tec5, Oberursel, Germany) UV/Vis spectrometer. Measurements were performed with a flashcounter of 20 and an average of 15 scans. For the determination of the extinction coefficient, a stock solution of EY in ethanol was prepared. From this a dilution series was prepared. Measurements were conducted using a standard 1 cm transmission cuvette (Hellma Analytics, Mülheim/R., Germany). From the measurement (Fig. S3), an extinction coefficient of $128381 \text{ L mol}^{-1} \text{ cm}^{-1}$ (at 520 nm) was obtained.

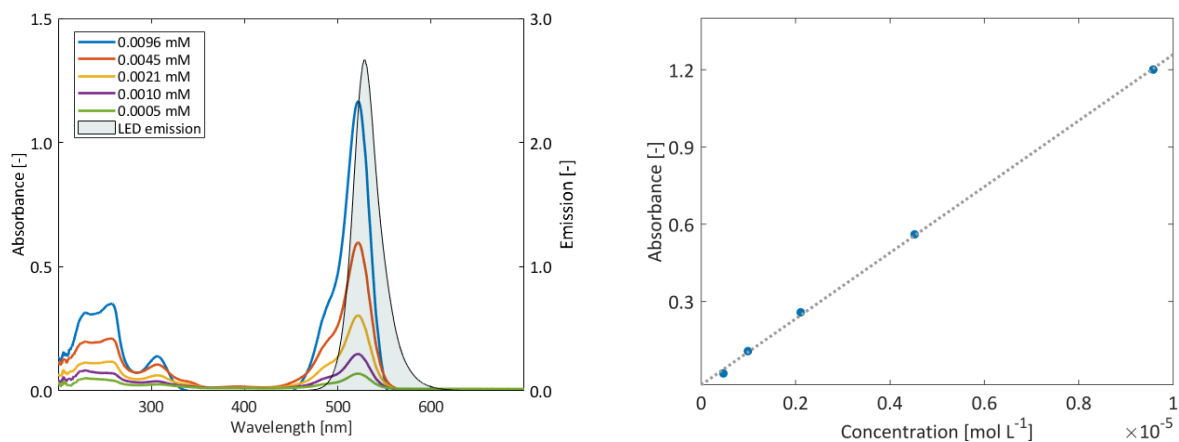


Fig. S3: Absorption spectra of an EY concentration series in ethanol and emission spectra of the used LED (left). Calculation of the absorption coefficient at the emission maximum of the used LED.

5. Feasibility Study

Both, the accuracy and the reliability of a chemometric model are based on the quality of the raw data. High signal to noise ratios and a minimum of signal overlapping mark a favorable starting position for further chemometric modeling. A first feasibility study revealed an overall weak sensitivity of UV/Vis spectroscopy towards the detection of 4-MTP and 4-MPD. Furthermore, the UV/Vis spectra were dominated by the catalyst fluorescence and therefore made the quantification not feasible. Both, in the mIR and Raman spectra, 4-MTP and 4-MPD showed characteristic bands in spectral region from 1000 to 1600 cm^{-1} . However, the signal intensity in the mIR spectra was comparably low and the spectra suffer from a strong signal overlap (Fig. S4). Even at the strongest band around 1244 cm^{-1} , a prediction model would operate at low accuracy due to the complete overlap and the minor difference in the peak wavenumber (around $\Delta 2 \text{ cm}^{-1}$). In the Raman spectra, both 4-MTP and 4-MPD could be differentiated in the spectral range of 1200 – 1000 cm^{-1} due to high signal intensity and an only weak signal overlap (Fig. S5). The additive TMEDA and the catalyst EY showed overall low signal intensity and was therefore not considered for further chemometric modelling.

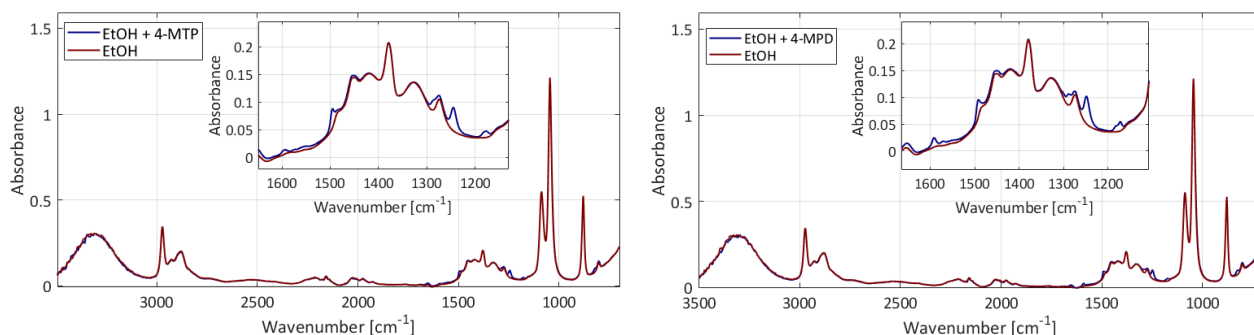


Fig. S4: mIR spectra of pure EtOH and binary mixtures containing EtOH/4-MTP (left) and EtOH/4-MPD (right) respectively.

Besides the considerations of the substrate and the product, the feasibility study in Raman spectroscopy also covered the potential influence from fluorescent species. Especially in photocatalytic reaction, the photosensitizer shows a strong fluorescent behavior.

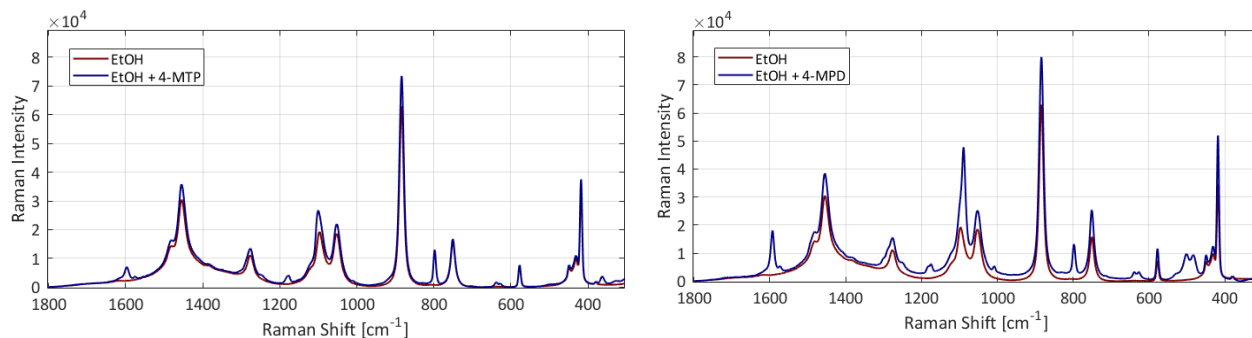


Fig. S5: Raman spectra of pure EtOH and binary mixtures containing EtOH/4-MTP (left) and EtOH/4-MPD (right) respectively.

In the case of an ethanolic EY solution it is clearly visible, that the laser induced fluorescence caused a stronger background intensity compared to the reference spectra of pure ethanol (Fig. S6). The fluorescent intensity is even increased when the Raman spectra is measured under reaction conditions (irradiation at 520 nm). However, the increase in the baseline intensity is weak enough to be subtracted by a linear baseline correction.

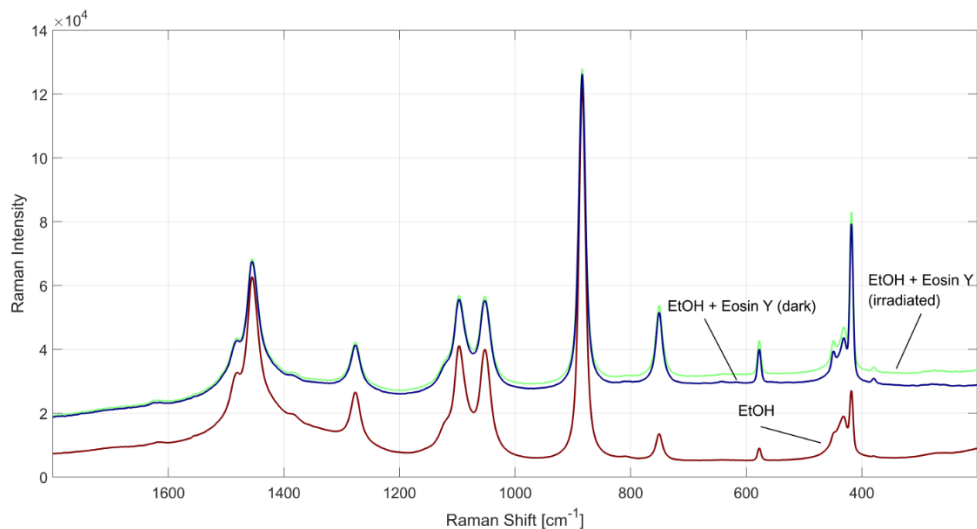


Fig. S6: Raman spectra of pure EtOH (brown) and in a mixture with the fluorescent dye EY under dark and illuminated conditions.

6. Fluorescence Quenching

Emission spectra were recorded using an AvaSpec 2048 (Avantes, Netherlands) UV/Vis spectrometer. As the excitation source, a green LED with an emission maximum of 520 nm was used. The integration time was set to 1000 ms with an average of 5.

For the emission measurement a stock solution of EY disodium salt in ethanol was prepared. From this, a dilution series was prepared in a way that the maximum absorption was below 0.1. The solution was degassed prior to the fluorescence measurements. Quenching studies were performed on 4-MTP and TMEDA. Using the Stern-Volmer equation (Eqn. S6.1) a molecular quenching constant K_{SV} of 7.28 and 0.92 was measured for 4-MTP and TMEDA respectively (Fig. S7).

$$\frac{I_0}{I} = 1 + K_{SV} \cdot [Q] \quad (\text{S6.1})$$

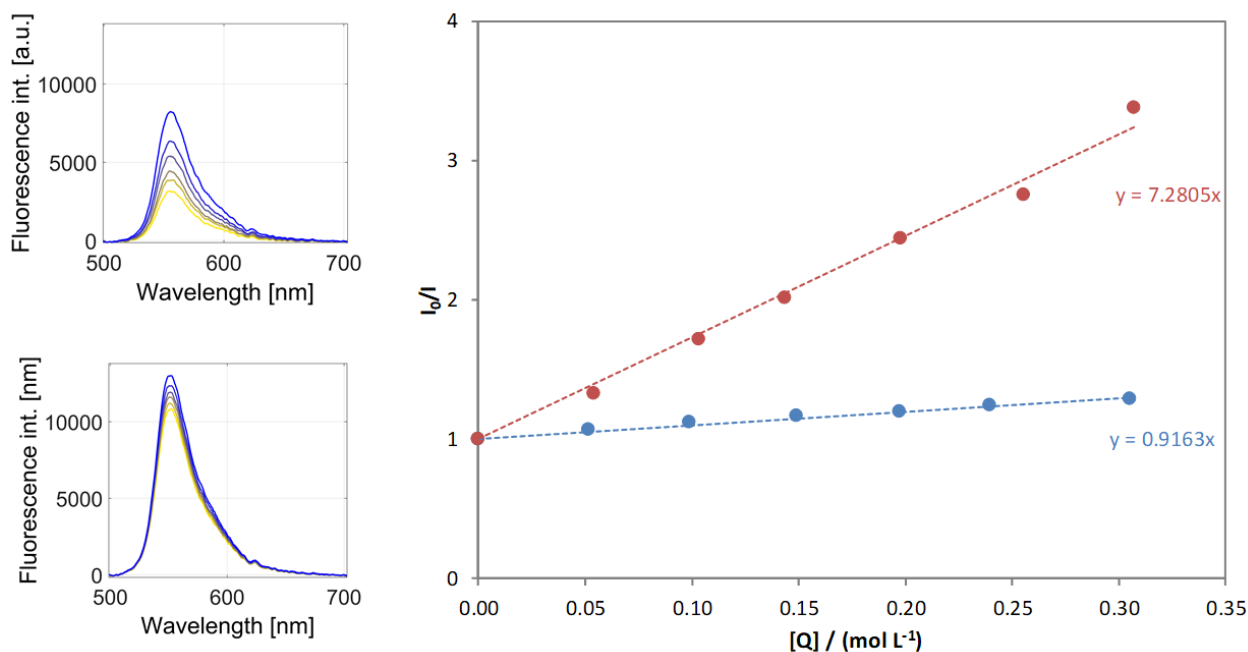


Fig. S7: Fluorescence quenching study of EY with 4-MTP (left, top) and TMEDA (left, bottom) as the quencher. Calculation of the quenching constant for 4-MTP (right, red) and TMEDA (right, blue).

7. Chemometric Modeling

a. Prediction Model

Chemometric modeling and spectra evaluation was performed using PEAXACT 4 (S-PACT, Aachen, Germany). Since the mixture spectra suffered from a strong signal overlapping in the most promising spectral range from 700 to 1200 cm^{-1} , a multivariate prediction model was necessary. By the help of an indirect hard modeling approach, the mixture spectrum was deconvoluted in its single components. By the help of a calibration the weighting of each component within the mixture is then correlated with the component concentration. To deal with the change in the background intensity, a data pretreatment was applied to all spectra (Fig. S8). The data pretreatment included a linear fit baseline subtraction and a peak normalization to the EtOH band at 880 cm^{-1} .

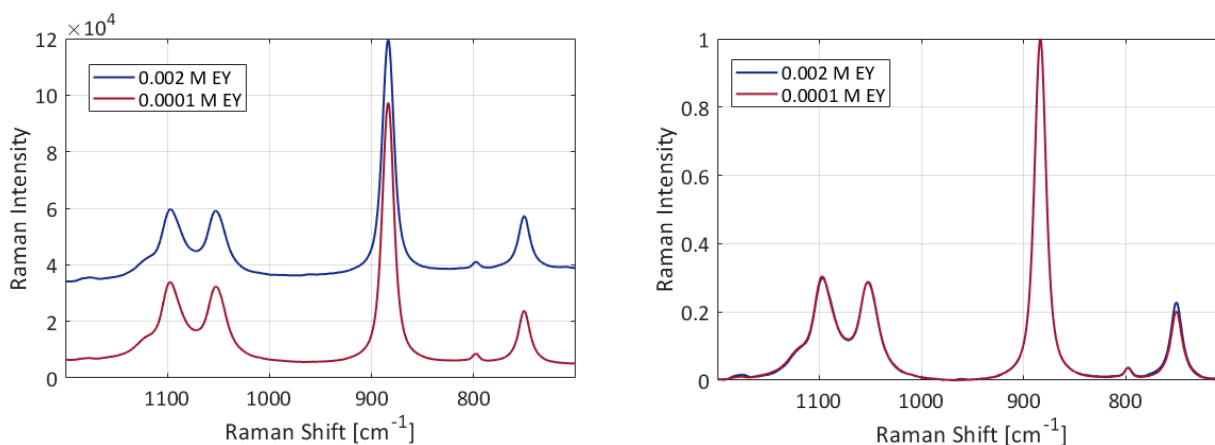


Fig. S8: Raman spectra of two representative samples with different EY loadings before (left) and after (right) data pretreatment.

The final model consists of four single component models representing the background, EtOH, 4-MTP and 4-MPD (Fig. S9). In the applied concentration range (up to 0.5 mM), EY showed no significant Raman band in the spectral range of 700-1200 cm^{-1} and was therefore not included in the prediction model. The additive TMEDA showed no characteristic band in the desired spectral range and was therefore also not considered in the prediction model. However, to test a possible impact on the accuracy of the final model, EY and TMEDA were used for the model validation. The final model was fitted to a representative Raman spectra that contained 4-MTP and 4-MPD in EtOH.

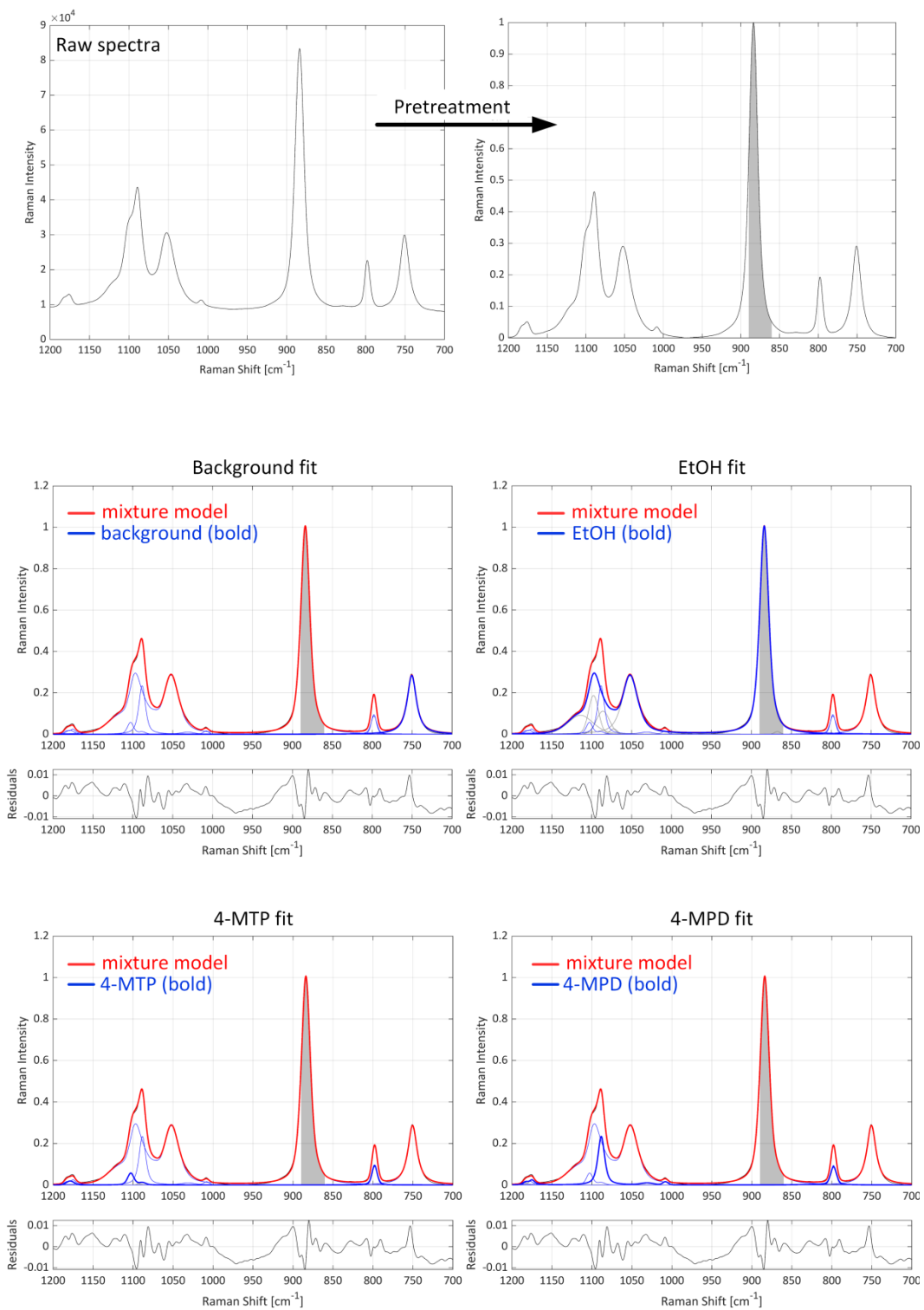


Fig. S9: Graphical representation of the contribution from each single component (blue) to the final mixture model (red) fitted to a representative mixture sample containing 4-MTP and 4-MPD in EtOH.

b. Model Calibration and Validation

The IHM was calibrated from gravimetrically prepared samples containing EtOH, 4-MTP and 4-MPD. In total 41 samples were used for the model calibration. In order to use an unbiased (certain degree of randomness) calibration set, ternary sample compositions were calculated with an iterative MATLAB routine according to the nearest neighbor statistic (Clark-Evans test).^[1] The nearest neighbor statistic is used to classify a data set as clustered ($R_n = 0$), random ($R_n = 1$) or regular ($R_n = 2.15$).

Within the predetermined calibration bounds (0 - 0.38 M MTP, 0 - 0.26 M MPD), a number of samples n was randomly generated. Afterwards the mean distance \bar{d} to the nearest neighbor was calculated for all points. The nearest neighbor statistic R_n is then calculated by comparing the observed mean distance to the regular case with equidistant points and no randomness in the total area a (Eqn. S7.1).

$$R_n = 2\bar{d} \frac{\sqrt{n}}{a} \quad (\text{S7.1})$$

If the new set of calibration samples had an improved nearest neighbor statistic (higher R_n value), it was counted as a successful iteration step. Iterative reconfiguration (15 cycles) led to the calibration set presented in Fig. S11 with no sample clustering and an appropriate range coverage.

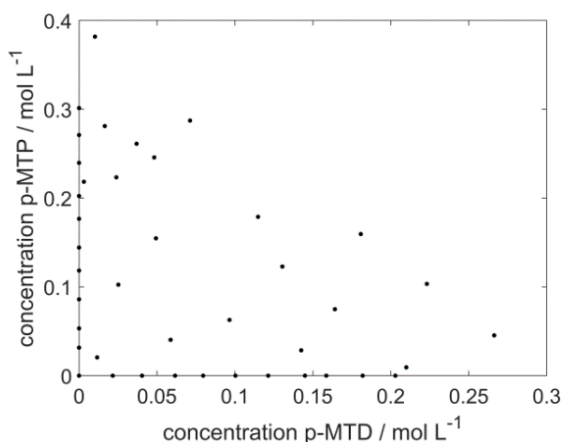


Fig. S10: Sample matrix used for the calibration of the IHM model.

[1] P.J. Clark., F.C. Evans, Ecology, 1954, **35**, 445-453.

Both, 4-MTP and 4-MPD were calibrated with a linear regression model (Fig. S11) to give reasonable R^2 values (Tab. S1).

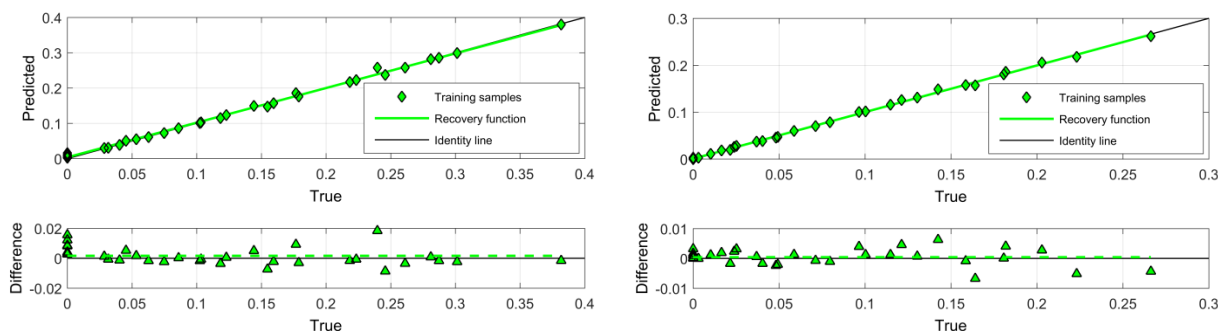


Fig. S11: Predicted vs true plot for the calibration of 4-MTP (left) and 4-MTP (right).

As the Raman spectra were affected by the EY fluorescence, the model was validated with representative reaction samples containing various amounts of EY (0.0001 M, 0.002 M and 0.06 M), TMEDA and the analyte (Fig. S12). The results show that the model is capable of predicting 4-MTP reliably even in the presence of a strong catalyst fluorescence. The validation revealed a reasonable RMSEP of 0.014 M for 4-MTP. Due to its overall higher signal intensity, 4-MPD was predicted with a higher accuracy (lower RMSEP) of 0.01 M.

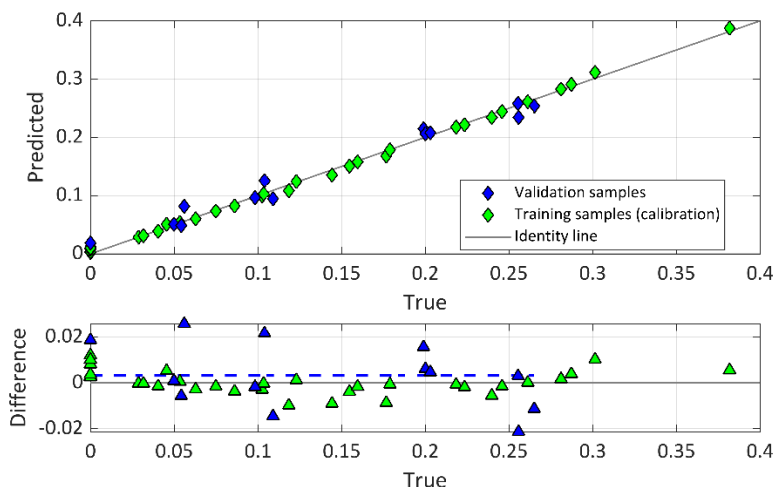


Fig. S12: Results of the model validation for 4-MTP.

Tab. S1: Results of the model calibration for 4-MTP and 4-MPD.

Component	4-MTP	4-MPD
Calibration Samples	41	41
Range	[0 0.3818]	[0 0.2663]
Calibration Function	linear	linear
R ²	0.997653	0.999304
RMSEC [mol L ⁻¹]	0.00521107	0.00199659
Bias C	0.000736133	0.000315596
RMSEP [mol L ⁻¹]	0.014	0.010

8. Oxygen Mass Transport

The oxygen concentration in the reaction samples is calculated based on its solubility properties in pure ethanol. For calculation, a molar fraction of 5.71×10^{-4} mol mol⁻¹ at 20 °C and a pressure of 1.013 bar was used.^[2] With this, the available oxygen concentration is calculated as 0.00978 mol L⁻¹ based on the molar mass ($M = 46.07$ g mol⁻¹) and density ($\delta = 0.789$ g mL⁻¹) of ethanol according to Eq. S8.1 .

$$c = x \cdot \frac{\rho_{ethanol}}{M_{ethanol}} \quad (S8.1)$$

Based on Henry's law, the Henry coefficient is given as 0.00965 mol L⁻¹ bar⁻¹.

$$K_H = \frac{c_{O_2}}{p_{O_2}} \quad (S8.2)$$

With this, the available oxygen content is calculated for the measured operating points in the interval of 0 – 3 bar.

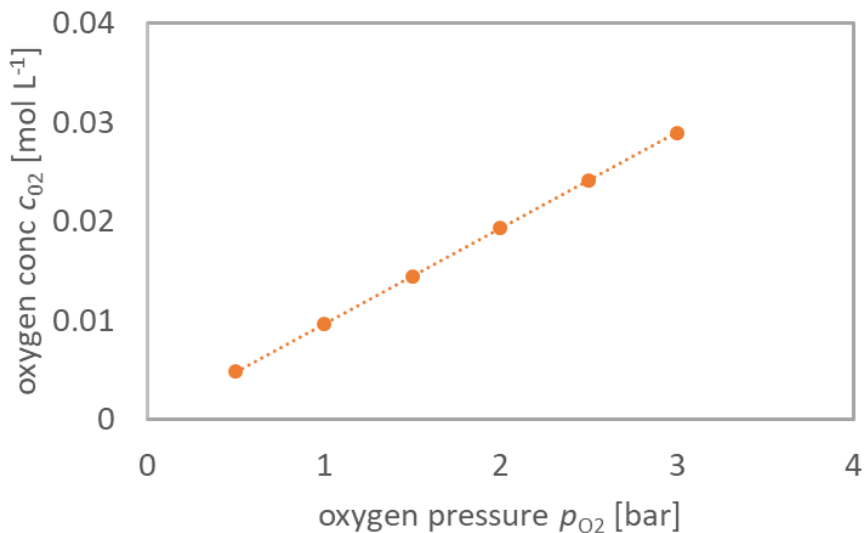


Fig. S13: Correlation of the dissolve oxygen concentration with the applied partial pressure according to Henry's law.

[2] T. Sato et al., *Ind. Eng. Chem. Res.* 2014, **53**, 19331–19337.

9. Catalyst Bleaching

a. General Information

During our investigation on the interplay of light intensity and catalyst concentration, a change in color was observed for some samples after irradiation (Fig. S14). Especially at low initial catalyst concentrations, the reaction solution underwent a full discoloration. With higher catalyst concentration the discoloration was less pronounced.



Fig. S14: Reaction samples before and after the irradiation.

To follow the discoloration during the reaction, we initially attempt to apply *in situ* UV/Vis spectroscopy. Utilizing an attenuated total reflection (ATR) immersion probe, UV/Vis spectra were recorded under process conditions. Unfortunately, the concentration of EY was below the detection limit of the measurement setup. Since the optical pathlength is significant lower in ATR measurements (typical in the nm range), the measurement setup was not capable of monitoring the EY absorption spectra. However, applying the ATR immersion probe to an ethanolic EY solution under external illumination allowed us to record *in situ* fluorescence spectra (Fig. S15). Interestingly, the fluorescence spectra from the *in situ* measurement differed from the standard offline measurement (see section 6 ESI).

b. Correlation of fluorescence maximum and EY concentration

As the spectral difference was assigned to the inner filter effect (IFE), we investigated various EY concentrations in the *in situ* setup ranging from 0 to 2.0×10^{-3} M. Increasing the EY concentration not only caused a weakening in the fluorescence intensity but also a bathochromic shift of the emission maximum from 540 nm to 580 nm (Fig. S13, left). Plotting the EY concentration against the corresponding wavelength of the emission maximum, an exponential correlation was obtained (Fig. S13, right). Fitting the data to an exponential model ($y = ax^b$), we obtained fitting parameters with a reasonable correlation coefficient ($R^2 = 0.998$; $a = 1.77E10^{-265}$; $b = 94.83$). With this equation in hand, the EY concentration could be predicted indirectly from its fluorescence spectra.

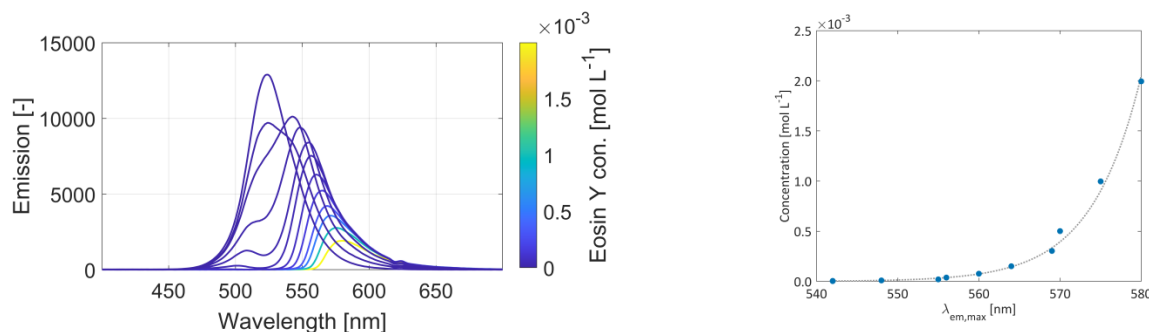


Fig. S15: Observed fluorescence intensity according to an increased EY concentration obtained from *in situ* measurements (left). Correlation of fluorescence maximum and EY concentration (right).

c. Fluorescence spectra in the course of the reaction

During the reaction, the fluorescence spectra were recorded by the previously described setup. Recording of the spectra was conducted using only the detection path of the probe connected to the spectrometer. The green activation light from the illumination unit was used as the excitation source. Exemplary spectra recorded during the reaction are shown in Fig. S16. The blue shift of the emission maxima is clearly visible.

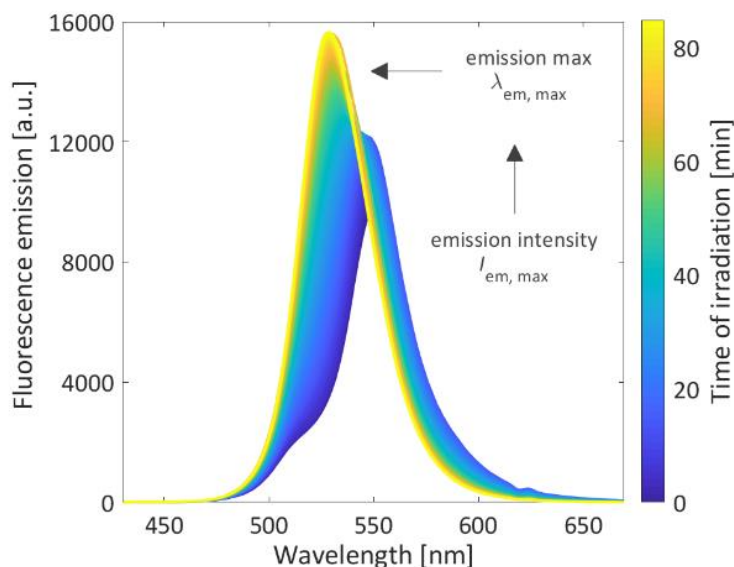


Fig. S16: *In situ* fluorescence spectra recorded during a photooxidation reaction.

d. Evaluation of the *in situ* fluorescence spectra

Based on these results, we simultaneously monitored the photooxidation of 4-MTP by *in situ* Raman and UV/Vis spectroscopy. Reactions were conducted at four different EY concentrations in a range of 0.005 to 0.04 mM. As expected, the emission maximum and its corresponding intensity changed throughout the reaction (Fig. S17). Upon closer inspection, it becomes apparent that, at the beginning of the reaction, the fluorescence intensity rises coherently with the reaction conversion (Fig. S17 top). We attributed this temporal change to the consumption of 4-MTP as the main fluorescence quencher. Upon reaching conversion rates exceeding 95 %, the trends in the fluorescence intensity differed depending on the initial EY concentration (Fig. S17 and S18). While a plateau

was found for the lowest initial EY concentration (orange), reactions conducted at higher concentrations (blue) showed a decrease in fluorescence intensity. Hence, indicating a loss in the active fluorophore due to the bleaching of EY. In this sense, the subsequent increase in fluorescence intensity for all reactions seemed counter intuitive. However, a deeper understanding of this can be obtained by looking at the temporal change in the position of the fluorescence maximum.

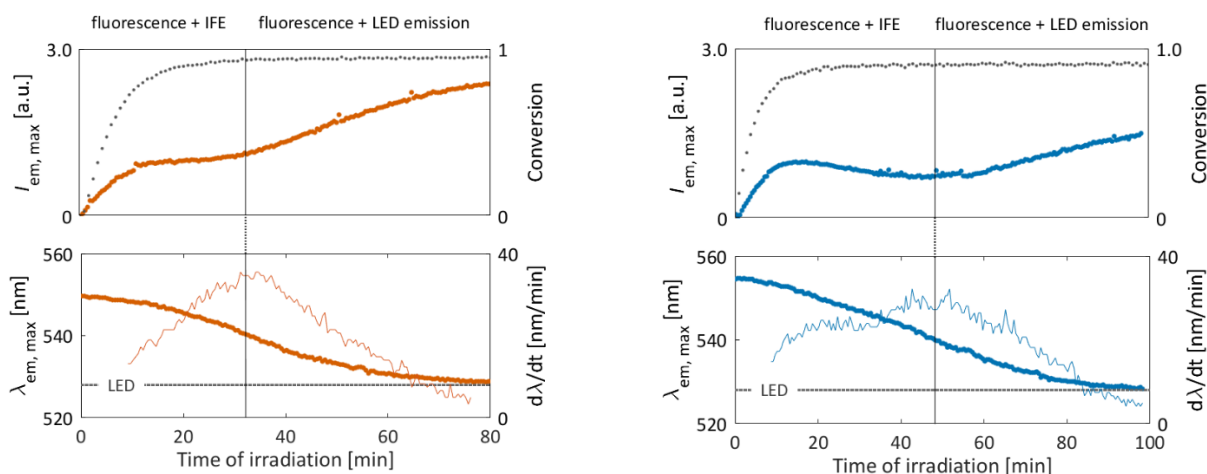


Fig. S17: Evaluation of the in situ fluorescence spectra for a reaction with an initial EY concentration of 0.005 mM (left) and 0.009 mM (right).

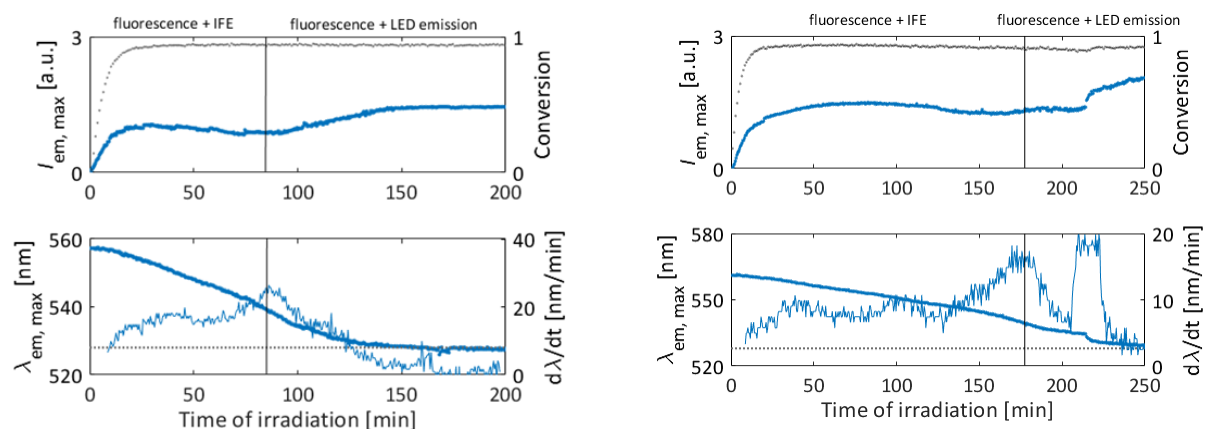


Fig. S18: Evaluation of the in situ fluorescence spectra for a reaction with an initial EY concentration of 0.019 mM (left) and 0.037 mM (right).

As shown in Fig. S17 and S18 (bottom), the emission maximum undergoes a continuous hypsochromic shift during the reaction. Starting from a maximum that depends on the initial EY concentration, all reactions show an asymptotically shift tending to 528 nm. Upon closer inspection, it becomes apparent that this wavelength matches the emission band of the used LED. Since only a spectrum in the absence of an absorbing or fluorescent species could represent the LED emission, almost full catalyst degradation is assumed upon reaching an emission maximum of 528 nm. The overall trend in the temporal change of the emission maximum resembled a sigmoidal behavior. As illustrated by the derivative in Fig. S17 and S18 (bottom), the inflection point shifts to higher irradiation times with the initial EY concentration. Interestingly, the corresponding emission maximum was found at 540 nm equally for all reactions. In fact, this wavelength represents the true emission of EY without any disturbing IFE and thus marking the lowest prediction limited of the IFE method. Based on this observation and the asymptotically behavior, it becomes evident that all trends observed below an emission maximum of 540 nm can be explained by a mixed state of remaining fluorescence and an increasing proportion of LED emission falling onto the probe.

e. Deconvolution of the fluorescence spectra

To resolve the contributions respectively, we again attempted to use an IHM approach. Treating both, the remaining fluorescence and the LED emission as a single component, the IHM reveals, albeit qualitatively, the further proceeding in EY bleaching (Fig. S19 and S20).

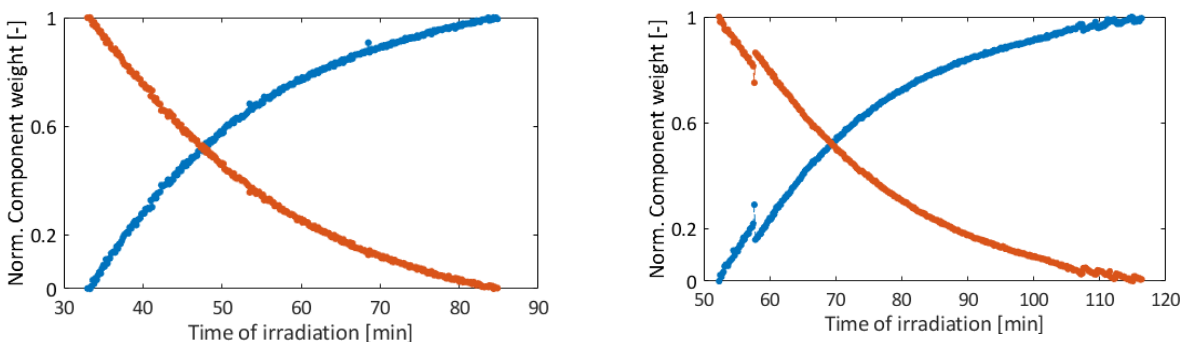


Fig. S19: Contribution of the remaining fluorescence (orange) and LED intensity (blue) to the measured fluorescence spectra for a reaction with an initial EY concentration of 0.005 mM (left) and 0.009 mM (right).

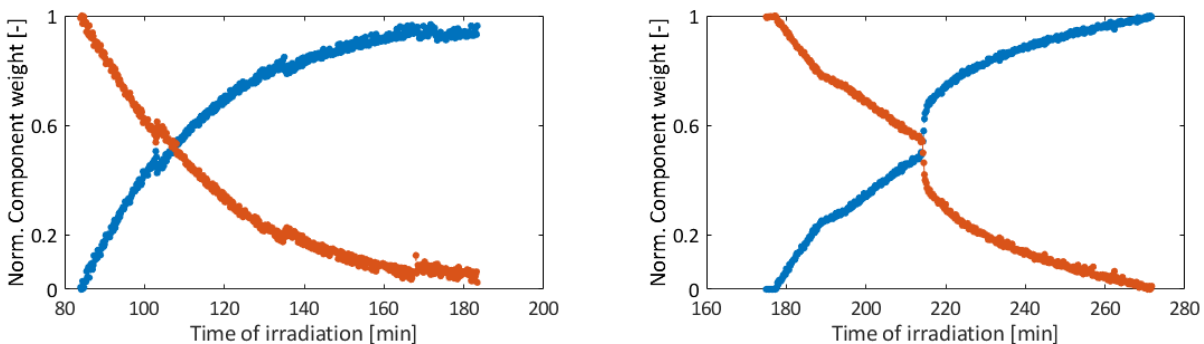


Fig. S20: Contribution of the remaining fluorescence (orange) and LED intensity (blue) to the measured fluorescence spectra for a reaction with an initial EY concentration of 0.019 mM (left) and 0.037 mM (right).

10. Interdependence of light intensity, EY concentration and photooxidation rate

a. Determination of light intensities

The light intensity within the reactor was measured using a radiometric calibrated UV/Vis spectrometer (Type T-UV-VIS-ES, Ocean Optics, Ostfildern, Germany). For the measurements a cosine corrector (type CC-3-UV-S, Ocean Optics, Ostfildern, Germany) with a collection angle of 180° and an active area of 3.8 mm^2 was used. The spectroradiometric calibration covered a wavelength region of 210 to 1050 nm. Light intensities were measured by averaging the spectral response from 200 to 850 nm. Measurements in the range of 10 to 100 % (according to the PWM input value) resulted in photon fluence rates ranging from 135 to $830 \text{ mol cm}^{-2} \text{ s}^{-1}$ (Fig. S21).

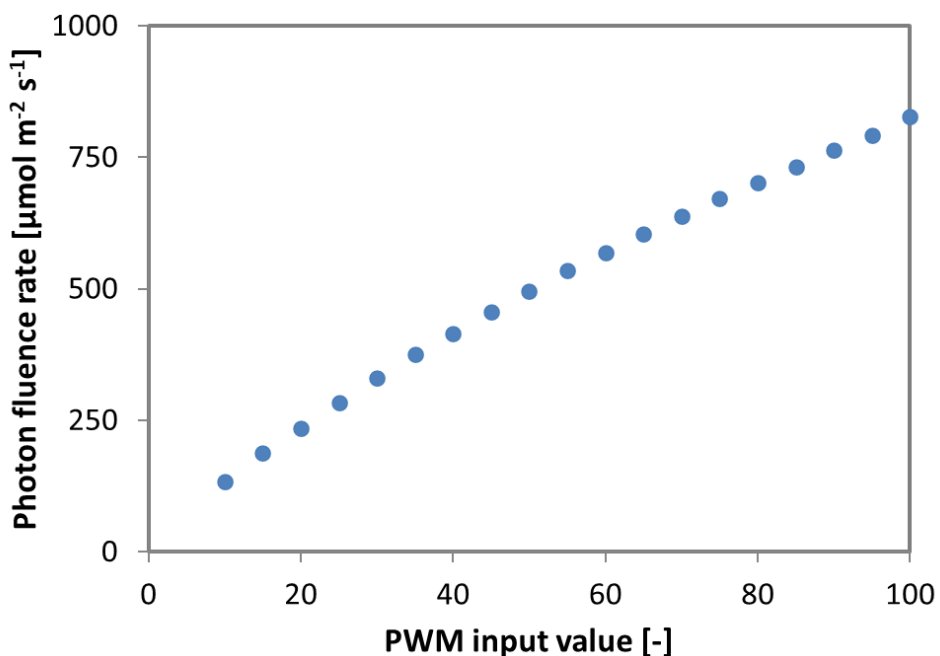


Fig. S21: Correlation of the PWM input value with the observed photon fluence rate within the reactor.

b. Simulation of the LVRPA

The simulation of the LVRPA at various photon fluence rates and EY concentrations was performed according to Eqn. S10.1 using an absorption coefficient of $128381 \text{ L mol}^{-1} \text{ cm}^{-1}$ (Fig. S22). For comparison, the dotted line represents the reactor depth of 0.58 cm.

$$\text{LVRPA} = I_0 \cdot \epsilon \cdot c_0 \cdot \ln(10) \cdot 10^{(-\epsilon \cdot c_0 \cdot z)} \quad (\text{S10.1})$$

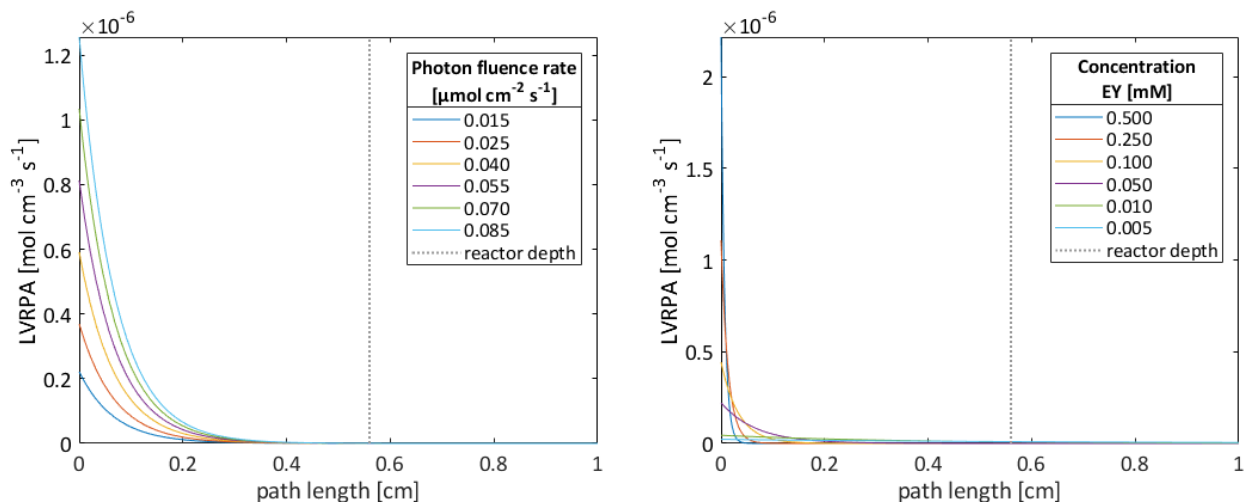


Fig. S22: Simulation of the LVRPA according to Eqn. 10.1 using an extinction coefficient of $128381 \text{ L mol}^{-1} \text{ cm}^{-1}$. Simulations were performed with an EY concentration of 0.05 mM (left) and a photon fluence rate of $150 \mu\text{mol m}^{-2} \text{ s}^{-1}$ (right).

c. Simulation of the AVRPA

The simulation of the AVRPA was performed according to Eqn. S10.2 using an absorption coefficient of $128381 \text{ L mol}^{-1} \text{ cm}^{-1}$ and a reactor depth of 0.58 cm (Fig. S23). The simulation clearly shows the linear dependence of the AVRPA with the photon fluence rate and the saturation behavior with the EY concentration. Upon a concentration of 0.04 mmol L^{-1} , the AVRPA becomes independent of the EY concentration.

$$\text{AVRPA} = \frac{1}{d} \int_0^d I_0 \cdot \epsilon \cdot c_0 \cdot \ln(10) \cdot 10^{(-\epsilon \cdot c_0 \cdot z)} dz = \frac{I_0 - I_0 10^{(-\epsilon \cdot c_0 \cdot d)}}{d} \quad (\text{S10.2})$$

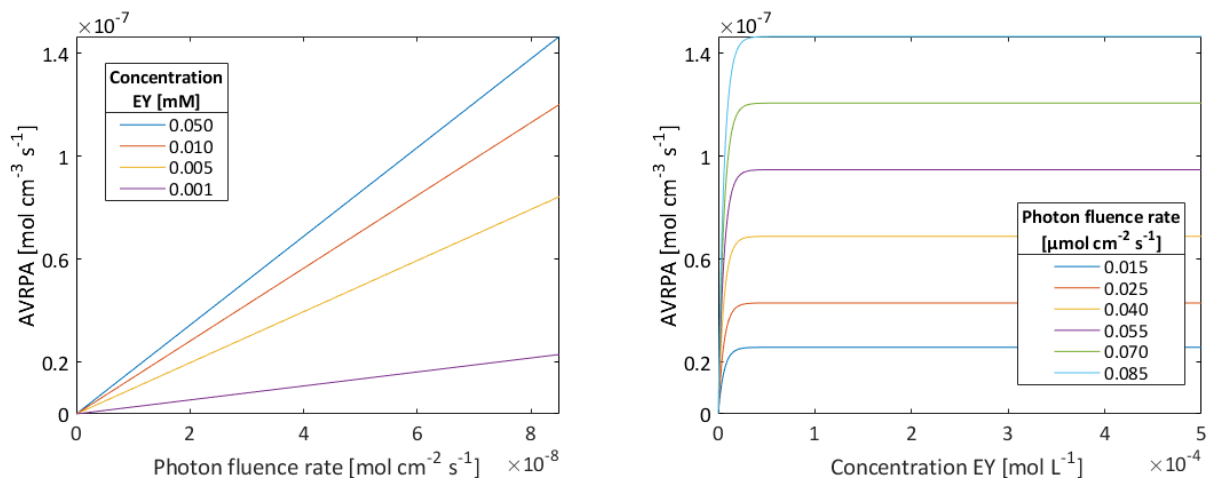


Fig. S23: Simulation of the AVRPA according to Eqn. 10.2 using and extinction coefficient of $128381 \text{ L mol}^{-1} \text{ cm}^{-1}$ and a reactor depth of 0.58 cm at a constant EY concentration (left) and a constant photon fluence rate (right).

d. Photooxidations under various EY concentrations

All reactions were performed in the previously described reactor setup at various EY concentrations in a range of 0 to 0.5 mM and a fixed photon fluence rate. All reactions were performed at a stirring speed of 1300 rpm and an oxygen pressure of 2 bar. Prior to irradiation all reaction mixtures were saturated with oxygen for 5 min. Evaluation with the IHM prediction model led to the initial photooxidation rates presented in Fig. S24.

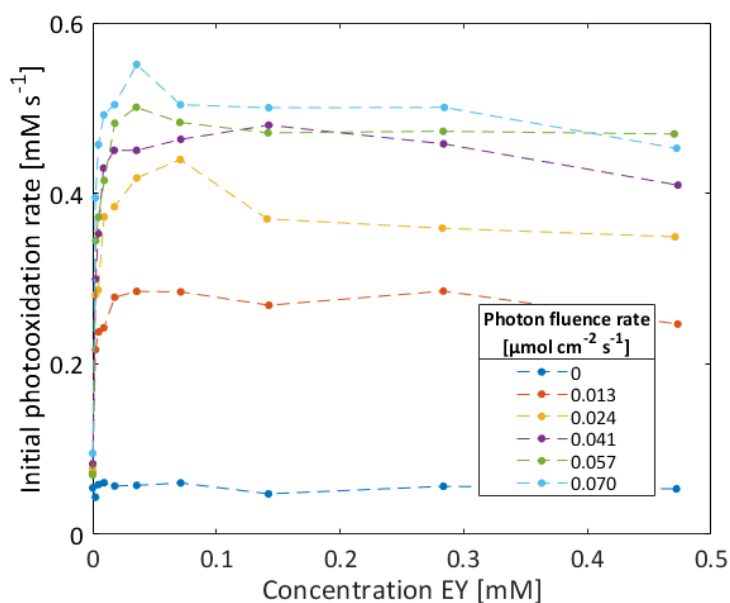


Fig. S24: Measured initial photooxidation rate at various EY concentrations and a fixed photon fluence rate.

e. Photooxidation under various photon fluence rates

All reactions were performed in the previously described reactor setup at various EY concentrations in a range of 0 to 0.5 mM at a fixed photon fluence rate. All reactions were performed at a stirring speed of 1300 rpm and an oxygen pressure of 2 bar. Prior to irradiation all reaction mixtures were saturated with oxygen for 5 Min. Evaluation with the IHM prediction model led to the initial photooxidation rates presented in Fig. S25.

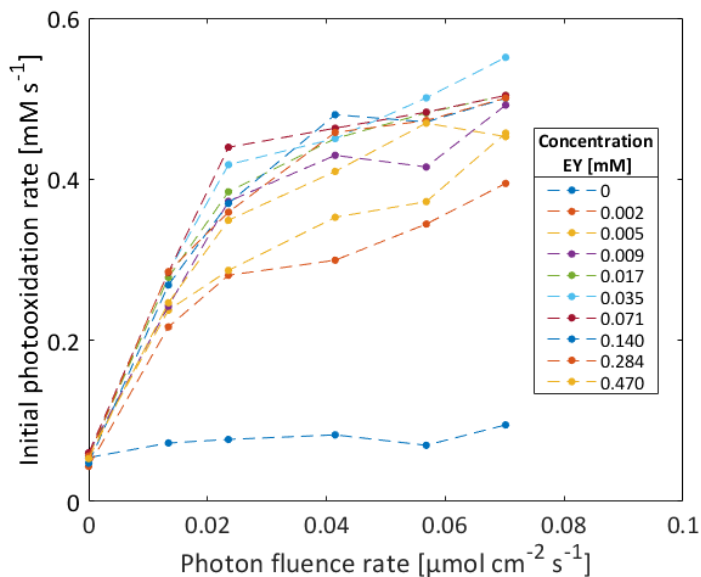


Fig. S25: Measured initial photooxidation rate at various photon fluence rates and fixed EY concentrations.

f. Kinetic evaluation

Based on the suggestion by Bloh^[3], we adopted the kinetic model to the photooxidation of 4-MTP. To obtain a kinetic rate law that describes the consumption of 4-MTP as a function of the applied AVRPA, we started from the catalytic cycle presented in Fig. S26. From this, the following rate laws were extracted. Assuming a steady state for EY, EY* and EY⁺ led to an expression for the temporal change in 4-MTP concentration (Eqn. 10.23)

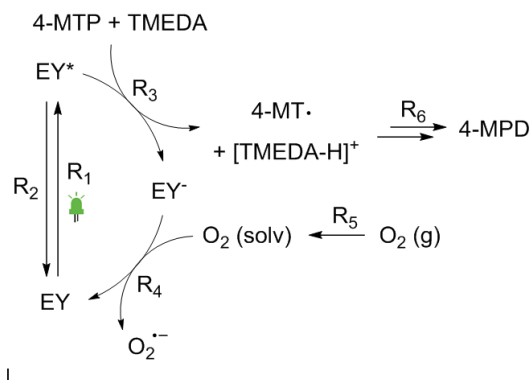


Fig. S26: Catalytic cycle for the photooxidation of 4-MTP with EY as the catalyst.

^[3] J. Z. Bloh, *Front. Chem.*, 2019, 7, 128.

$$\frac{d[\text{EY}]}{dt} = -R1 + R2 + R4 \quad (\text{S10.3}) \quad R1 = k1 \frac{[\text{EY}]}{[\text{EY}]_{\text{total}}} \quad (\text{S10.10})$$

$$\frac{d[\text{EY}^*]}{dt} = R1 - R2 - R3 \quad (\text{S10.4}) \quad R2 = k2 [\text{EY}^*] \quad (\text{S10.11})$$

$$\frac{d[\text{EY}^-]}{dt} = R3 - R4 \quad (\text{S10.5}) \quad R3 = k3 [\text{EY}^*][4\text{MTP}] \quad (\text{S10.12})$$

$$\frac{d[4\text{MTP}]}{dt} = -R3 \quad (\text{S10.6}) \quad R4 = k4 [\text{EY}^-][\text{O}_2(\text{g})] \quad (\text{S10.13})$$

$$\frac{d[\text{MT} \cdot]}{dt} = R3 \quad (\text{S10.7}) \quad R5 = k5 [\text{O}_2(\text{g})] \quad (\text{S10.14})$$

$$\frac{d[4\text{MPD}]}{dt} = R6 \quad (\text{S10.8}) \quad R6 = k6 [\text{MT} \cdot]^2 \quad (\text{S10.15})$$

$$\frac{d[\text{O}_2(\text{solv})]}{dt} = R5 - R4 \quad (\text{S10.9})$$

$$k1 = \phi L_p^a \quad (\text{S10.16}) \quad R1 = R2 + R3 \quad (\text{S10.19})$$

$$k2 = \frac{1}{\tau} \quad (\text{S10.17}) \quad R1 = R2 + R4 \quad (\text{S10.20})$$

$$L_p^a(z) = \epsilon [\text{EY}]_{\text{total}} \ln(10) I_0 10^{-\epsilon [\text{EY}]z} \quad (\text{S10.18}) \quad R3 = R4 \quad (\text{S10.21})$$

$$[\text{EY}]_{\text{total}} = [\text{EY}] + [\text{EY}^*] + [\text{EY}^-] \quad (\text{S10.22})$$

With a steady state consumption, the following rate laws were obtained:

$$\frac{d[\text{EY}]}{dt} = -k1 \frac{[\text{EY}]}{[\text{EY}]_{\text{total}}} + k2 [\text{EY}^*] + k4 [\text{EY}^-][\text{O}_2(\text{solv})] \approx 0$$

$$\frac{d[\text{EY}^*]}{dt} = k1 \frac{[\text{EY}]}{[\text{EY}]_{\text{total}}} - k2 [\text{EY}^*] - k3 [\text{EY}^*][4\text{MTP}] \approx 0$$

$$\frac{d[\text{EY}^-]}{dt} = k3 [\text{EY}^*][4\text{MTP}] - k4 [\text{EY}^-][\text{O}_2(\text{solv})] \approx 0$$

With these rate laws the consumption of 4-MTP could be described as a function of the initial EY concentration and the photo fluence rate (Eqn. S10.23).

$$\frac{d[\text{EY}^*]}{dt} = 0 = k_1 \frac{[\text{EY}]}{[\text{EY}]_{\text{total}}} - k_2 [\text{EY}^*] - k_3 [\text{EY}^*][4\text{MTP}]$$

$$\Leftrightarrow k_1 \frac{[\text{EY}]}{[\text{EY}]_{\text{total}}} = k_2 [\text{EY}^*] + k_3 [\text{EY}^*][4\text{MTP}]$$

$$\Leftrightarrow [\text{EY}] = \frac{[\text{EY}]_{\text{total}}}{k_1} (k_2 [\text{EY}^*] + k_3 [\text{EY}^*][4\text{MTP}])$$

$$\frac{d[\text{EY}^-]}{dt} = 0 = k_3 [\text{EY}^*][4\text{MTP}] - k_4 [\text{EY}^-][\text{O}_2(\text{soln})]$$

$$\Leftrightarrow k_4 [\text{EY}^-][\text{O}_2(\text{soln})] = k_3 [\text{EY}^*][4\text{MTP}]$$

$$\Leftrightarrow [\text{EY}^-] = \frac{k_3 [\text{EY}^*][4\text{MTP}]}{k_4 [\text{O}_2(\text{soln})]}$$

$$[\text{EY}]_{\text{total}} = [\text{EY}] + [\text{EY}^*] + [\text{EY}^-]$$

$$[\text{EY}]_{\text{total}} = \frac{[\text{EY}]_{\text{total}}}{k_1} (k_2 [\text{EY}^*] + k_3 [\text{EY}^*][4\text{MTP}]) + [\text{EY}^*] + \frac{k_3 [\text{EY}^*][4\text{MTP}]}{k_4 [\text{O}_2(\text{soln})]}$$

$$[\text{EY}]_{\text{total}} = \frac{k_2}{k_1} k [\text{EY}]_{\text{total}} [\text{EY}^*] + \frac{k_3}{k_1} [\text{EY}]_{\text{total}} [\text{EY}^*][4\text{MTP}] + [\text{EY}^*] + \frac{k_3 [\text{EY}^*][4\text{MTP}]}{k_4 [\text{O}_2(\text{soln})]}$$

$$[\text{EY}]_{\text{total}} = [\text{EY}^*] \left(\frac{k_2}{k_1} k [\text{EY}]_{\text{total}} + \frac{k_3}{k_1} [\text{EY}]_{\text{total}} [4\text{MTP}] + 1 + \frac{k_3 [4\text{MTP}]}{k_4 [\text{O}_2(\text{soln})]} \right)$$

$$[\text{EY}^*] = \frac{[\text{EY}]_{\text{total}}}{\frac{k_2}{k_1} k [\text{EY}]_{\text{total}} + \frac{k_3}{k_1} [\text{EY}]_{\text{total}} [4\text{MTP}] + 1 + \frac{k_3 [4\text{MTP}]}{k_4 [\text{O}_2(\text{soln})]}}$$

$$[\text{EY}^*] = \frac{[\text{EY}]_{\text{total}}}{\frac{k_2 [\text{EY}]_{\text{total}} + k_3 [\text{EY}]_{\text{total}} [4\text{MTP}]}{k_1} + 1 + \frac{k_3 [4\text{MTP}]}{k_4 [\text{O}_2(\text{soln})]}}$$

$$\frac{d[4\text{MTP}]}{dt} = - \frac{k_3 [\text{EY}]_{\text{total}} [4\text{MTP}]}{\frac{k_2 [\text{EY}]_{\text{total}} + k_3 [4\text{MTP}] [\text{EY}]_{\text{total}}}{k_1} + 1 + \frac{k_3 [4\text{MTP}]}{k_4 [\text{O}_2(\text{soln})]}}$$

$$\frac{d[4\text{MTP}]}{dt} = - \frac{k3[\text{EY}]_{\text{total}} [4\text{MTP}]}{\frac{k2 [\text{EY}]_{\text{total}} + k3[4\text{MTP}] [\text{EY}]_{\text{total}}}{\phi L_p^a} + 1 + \frac{k3 [4\text{MTP}]}{k4[\text{O}_2(\text{solv})]}}$$

$$\frac{d[4\text{MTP}]}{dt} = - \frac{k3[\text{EY}]_{\text{total}} [4\text{MTP}]}{\frac{k2 [\text{EY}]_{\text{total}} + k3[4\text{MTP}] [\text{EY}]_{\text{total}}}{\phi \epsilon [\text{EY}]_{\text{total}} \ln(10) I_0 10^{-\epsilon[\text{EY}]z}} + 1 + \frac{k3 [4\text{MTP}]}{k4[\text{O}_2(\text{solv})]}}$$

$$\frac{d[4\text{MTP}]}{dt} = - \frac{k3[\text{EY}]_{\text{total}} [4\text{MTP}]}{\frac{k2 + k3[4\text{MTP}]}{\phi \epsilon \ln(10) I_0 10^{-\epsilon[\text{EY}]_{\text{total}}z}} + 1 + \frac{k3 [4\text{MTP}]}{k4[\text{O}_2(\text{solv})]}} \quad (\text{S10.23})$$

g. Simulation of <r>

Based on Eqn. S10.23 the response of the initial photooxidation rate was simulated using MATLAB. Since the reaction rate was found to be a function of the absorbed photon flux, it also becomes a function of the position within the reactor. Consequently, the measured reaction rate must be understood as an averaged reaction rate. The averaged reaction rate is obtained from integrating Eqn. 23 over the reaction volume. Simulation with MATLAB of the resulting averaged reaction rate at various AVRPA values gave a linear correlation (Fig. S26). For the simulation, parameters listed in Tab. S2 were used.

Correction of Eqn. 23 considering local differences in an effective quantum yield led to the observed logarithmic behavior (Fig. S26).

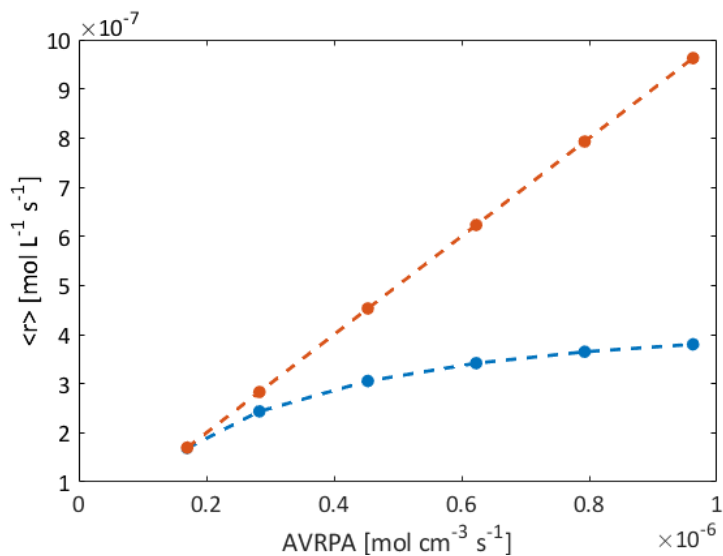


Fig. S26: Simulation of the averaged reaction rate with (orange) and without (blue) correction of a local dependent effective quantum yield.

Tab. S2: Used variables for the simulation of the averaged reaction rate considering an effective quantum yield.

k2	$3 \times 10^{-9} \text{ s}^{-1}$
K3	$1 \times 10^{-10} \text{ L mol}^{-1} \text{ s}^{-1}$
K4	$1 \times 10^{-10} \text{ L mol}^{-1} \text{ s}^{-1}$
c(MTP)	0.2 mol L^{-1}
C(O2)	0.02 mol L^{-1}
ϵ	$128381 \text{ L mol}^{-1} \text{ cm}^{-1}$
Dreact	0.1
LVRPAcrit	$4 \times 10^{-7} \text{ mol cm}^{-3} \text{ s}^{-1}$
Φ_{max}	2.5

h. Error estimation

From the model validation, a RMSEP of 0.014 and 0.01 was determined for 4-MTP and 4-MPD, respectively. The initial photooxidation rate r was calculated by numerical differentiation of the measured concentration-time profile according to Eqn. S10.24. Assuming that the concentration values are independent variables (single Raman measurements) and the time is measured without a significant error, the uncertainty on the calculated initial rate σ_r can be obtained from Eqn. S10.25.

$$r = \frac{c_{4\text{MTP},t_2} - c_{4\text{MTP},t_1}}{t_2 - t_1} \quad (\text{S10.24})$$

$$\sigma_r = \sqrt{\left(\frac{\partial r}{\partial c_{4\text{MTP},t_1}}\right)^2 \cdot \sigma_{c(4\text{-MTP}),t_1}^2 + \left(\frac{\partial r}{\partial c_{4\text{MTP},t_2}}\right)^2 \cdot \sigma_{c(4\text{MTP}),t_2}^2} \quad (\text{S10.25})$$

Using the RMSEP as the error on the concentration, the uncertainty on the reaction rate is calculated from Eqn. S10.26.

$$\sigma_r = \sqrt{\text{RMSEP}^2 \left[\left(\frac{1}{t_2 - t_1}\right)^2 + \left(\frac{1}{t_1 - t_2}\right)^2 \right]}$$

$$\sigma_r = \sqrt{\frac{2 \cdot \text{RMSEP}^2}{\Delta t^2}}$$

$$\sigma_r = \sqrt{2} \cdot \frac{\text{RMSEP}}{\Delta t} \quad (\text{S10.26})$$

With a RMSEP of 0.014 M and a time interval of 3.7 min, a moderate uncertainty of 0.005 M min⁻¹ is calculated on the initial oxidation rate. Since only minor fluctuations in the concentration-time profiles were observed, using the RMSEP as the error on the concentration might be an overestimation.